Monthly Notices
of the
ROYAL ASTRONOMICAL SOCIETY

MNRAS **491,** 5572–5578 (2020) doi:10.1093/mnras/stz3238

Spectral characteristic of mid-term quasi-periodicities in sunspot data

P. Frick [1,2★] D. Sokoloff,[1,3,4] R. Stepanov [1,5] V. Pipin [6] and I. Usoskin [7]

[1] *Institute of Continuous Media Mechanics, Korolyov str. 1, 614013 Perm, Russia*
[2] *Perm State University, Bukireva str. 15, 614990 Perm, Russia*
[3] *Department of Physics, Moscow University, 119899 Moscow, Russia*
[4] *IZMIRAN, Kaluzhskoe shasse, 4, Troitsl, 108840 Moscow, Russia*
[5] *Perm National Research Polytechnic University, 614990 Perm, Russia*
[6] *Institute of Solar-Terrestrial Physics, 664030 Irkutsk, Russia*
[7] *University of Oulu, 90014 Oulu, Finland*

Accepted 2019 November 14. Received 2019 October 9; in original form 2019 July 22

ABSTRACT

Numerous analyses suggest the existence of various quasi-periodicities in solar activity. The power spectrum of solar activity recorded in sunspot data is dominated by the ∼11-yr quasi-periodicity, known as the Schwabe cycle. In the mid-term range (1 month–11 yr) a pronounced variability known as a quasi-biennial oscillation is widely discussed. In the shorter time-scale a pronounced peak, corresponding to the synodic solar rotation period (∼27 d), is observed. Here we revisit the mid-term solar variability in terms of statistical dynamics of fully turbulent systems, where solid arguments are required to accept an isolated dominant frequency in a continuous (smooth) spectrum. For this, we first undertook an unbiased analysis of the standard solar data, sunspot numbers and the F10.7 solar radio flux index, by applying a wavelet tool, which allows one to perform a frequency–time analysis of the signal. Considering the spectral dynamics of solar activity cycle by cycle, we showed that no single periodicity can be separated, in a statistically significant manner, in the specified range of periods. We examine whether a model of the solar dynamo can reproduce the mid-term oscillation pattern observed in solar data. We found that a realistically observed spectrum can be explained if small spatial (but not temporal) scales are effectively smoothed. This result is important because solar activity is a *global* feature, although monitored via small-scale tracers like sunspots.

Key words: Sun: activity – sunspots – methods: data analysis – dynamo.

1 INTRODUCTION

Cyclic solar activity is mostly presented by the dominant famous ∼11-yr cycle known as the Schwabe cycle. This cycle was discovered in the 19th century via a simple analysis of sunspot numbers, but it is also apparent in other tracers of solar activity. The origin of the cycle is believed to be associated with the solar dynamo action. More specifically, the Schwabe cycle is understood as a leading eigensolution of solar dynamo equations. Using different magnetic tracers, solar physicists found that the cycle is formed by propagation of a wave of quasi-stationary magnetic field and that it is in fact a 22-yr magnetic cycle, which is observed as an 11-yr one because the sunspot number is insensitive to the sign of the magnetic field.

The variability of solar activity is, however, much more complex than just the Schwabe cycle. Analyses of sunspot data undertaken by many researchers (for reviews see e.g. Hathaway 2015; Usoskin 2017) suggested that various periods exist in solar variability. Some of these periods are longer than the Schwabe cycle (e.g. the Gleissberg cycle, with a typical time-scale of about 100 yr) while others are shorter. Most discussed quasi-periodic cycles in the mid-term range are attributed to oscillations on about a 2-yr time-scale (e.g. Benevolenskaya 1995), called the quasi-biennial oscillation (QBO). It was shown later that QBO corresponds to a wide range of periods (0.6–4 yr according to Bazilevskaya et al. 2014) and behaves intermittently. QBO has also been referred to as intermediate or mid-term quasi-periodicities, identified with particular spectral peaks. However, this definition obviously deserves further clarification and discussion. If accepted naively, it reads that the period of oscillation varies with a characteristic time, which is substantially larger than the nominal period. This is likely the case when the

★ E-mail: rodion@icmm.ru

original definition is misleading, and new concepts are required. We note that this is not solely a problem of terminology, since sunspot data and their interpretation form the basis of solar dynamo studies, where periodicities are associated with eigenfrequencies of the solar dynamo.

Several physical mechanisms have been proposed to explain the QBO (e.g. Fletcher et al. 2010; Zaqarashvili et al. 2010; Simoniello et al. 2013; Dikpati et al. 2018). Inceoglu et al. (2019) demonstrated that, while some contemporary detailed dynamo models can yield oscillations similar to the QBO, others do not, which makes QBO a kind of test for different dynamo models. We suggest a revised physical explanation of the QBO phenomenon observed in the mid-term range of sunspot variations.

From the point of view of large-scale dynamics, the Sun is a very complicated magneto-hydrodynamical system operating under large values of the control parameters (Reynolds, Grashof, Hartmann numbers), in which the largest (lowest in Fourier space) modes appear on the background of fully developed turbulent media. A similar problem of identification of quasi-stable oscillations in turbulent systems is typical for fluid dynamics.

It is worth noting that the discovery of large-scale flow (convective wind; see e.g. Krishnamurti & Howard 1981; Busse 1983) in fully developed convective systems in the laboratory (notably at much more moderate scales and parameters than solar plasma) was recognized by the community with some scepticism. It took time to bring the study of the dynamics of large-scale circulation into the separate topic of Rayleigh–Bénard convection (Ahlers, Grossmann & Lohse 2009). The first attempts to study the temporal dynamics of large-scale modes in a convective cell revealed a complex spectrum with a series of peaks (Bogatyrev, Gilev & Zimin 1980). Similar features were detected in the space–time spectra (that is, the temporal spectra of the isolated spatial mode) of various turbulent hydrodynamic systems and suggested similarities with the data on solar-related periodicities (Zimin & Frick 1988). However, attempts to obtain reliable sequences in long-running (several weeks) laboratory experiments showed that as soon as statistics become reliable (the sample coverage greatly exceeds the characteristic times studied), the spectra become smooth and only one dominant frequency survives in some cases (Niemela et al. 2001; Qiu & Tong 2001; Vasiliev et al. 2016).

In this paper we suggest, based on the background of turbulent and convection studies, that the mid-term (0.1–11 yr) solar dynamics should be considered in terms of the statistical dynamics of fully turbulent systems. Otherwise convincing physical arguments or robust statistics are required to distinguish a dominant frequency in a continuous spectrum.

For this, we first undertake an unbiased analysis of the standard solar data, namely, sunspot number, considering the spectral dynamics of solar activity cycle by cycle. The results of the analysis were also verified with the F10.7 cm solar radio flux index. As a spectral tool we use a wavelet analysis, which is helpful in studies of solar variability (e.g. Lawrence, Cadavid & Ruzmaikin 1995; Frick et al. 1997). We then apply a simplified non-axisymmetric model of the solar dynamo to reproduce the observed spectral statistics in the mid-term range.

2 DATA

We based our analysis on sunspot activity as quantified in several indices. We analysed the international total sunspot number (ISN, v.2.0, Clette & Lefèvre 2016), which is based on the classical Wolf sunspot number series with correction of some apparent errors and

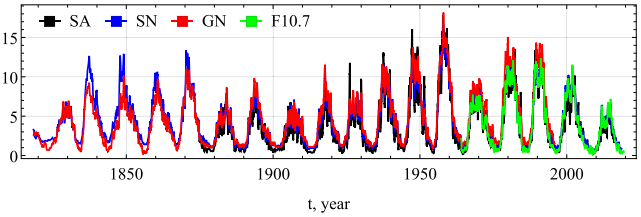

Figure 1. Datasets used in this work: sunspot area (SA, black, normalized by a factor of 226), sunspot number (SN, blue, normalized by 20.01), sunspot group number (GN, red, normalized by 20.01), the solar radio flux in the wavelength 10.7 cm (F10.7, green, normalized by 20.01).

recalibration to Wolfer as the reference observer. Sunspot number represents a synthetic number, being a combination of the weighted number of sunspot groups and the number of individual spots, corrected for the individual observer's quality factor. Henceforth it is called the SN series. The data are available from the SILSO database http://www.sidc.be/silso/datafiles.

We also considered the sunspot group number (henceforth GN), which provides the number of sunspot groups visible on the solar disc at a given time. This series was obtained by Usoskin et al. (2016) using the active-day-fraction method from the raw database of sunspot group observations (Vaquero et al. 2016) for the period 1749–1995. This dataset is available at http://www.sidc.be/silso/DATA/GroupNumber/GNiu_d.txt.

We also considered the sunspot area (henceforth SA) as observed by the Royal Greenwich Observatory (RGO) for the period 1876–1976 and extended after 1976 by the USAF/NOAA dataset scaled with the factor 1.4. Both hemispheric and global sunspot areas were used. The dataset and its full description can be found at https://solarscience.msfc.nasa.gov/greenwch.shtml (see also Hathaway 2015).

In addition, we also considered the F10.7 solar index, which is the solar radio flux in the wavelength 10.7 cm (2800 MHz) originating from the upper chromosphere/lower corona. This forms one of the longest directly measured (in contrast to synthetic sunspot data) solar indices and has been available since the mid-20th century. The dataset was obtained from the OMNIWeb data service (https://omniweb.gsfc.nasa.gov).

We used daily data, which is the best cadence for this type of data, but we appreciate that the sunspot's lifetime is longer (days to weeks for individual spots and months for an active region), so that the results of our analysis (especially at time-scales comparable with the spot lifetime) can be determined by both the dynamo mechanism of cyclic solar magnetic activity and the physics of sunspot/active-region evolution.

The time series used here are shown in Fig. 1. We note that each dataset covers a specific time interval. As the datasets deal with slightly different kind of tracers, normalization is required to make the results of our analysis comparable. We use the following normalizations: SN, GN and F10.7 are normalized by a factor of 20.01, and SA is normalized by 226.

The solar dynamo produces two 11-yr periodic activity waves, one in each hemisphere. In principle, the periodicities under discussion might be associated with activity waves in a particular hemisphere. To test this option we analyse additionally the datasets for particular hemispheres separately. All the datasets used provide an indication of the hemisphere where a particular sunspot is located. As an example, we show in Fig. 2 time series of sunspot areas separated by hemispheres in comparison with total data.

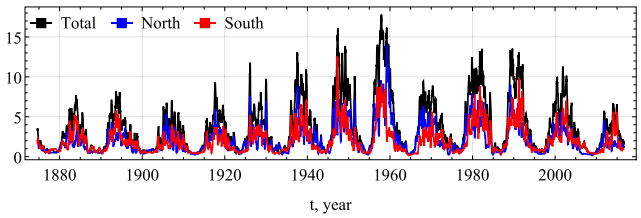

Figure 2. Time series for sunspot area (SA), normalized by a factor of 226: total (black), Northern hemisphere (blue), Southern hemisphere (red).

3 WAVELETS

Our aim is to identify quasi-periodic components in a stochastic and noisy signal, considering that both the period and amplitude of oscillations may vary from cycle to cycle (Hathaway 2015). There is a suitable mathematical tool for such an analysis known as wavelet analysis (e.g. Mallat 2008), which is a localized version of Fourier analysis: the analysed signal is compared with a wave packet of various wavelengths centred at various times. Wavelets have been successfully used to analyse sunspot data since the first studies by Lawrence et al. (1995), Nesme-Ribes et al. (1995).

In general, various profiles of wave packets may be exploited, but here we use harmonic oscillations modulated by a Gaussian envelope (the so-called Morlet wavelet),

$$\psi(t) = \sigma^{-1/2} \mathrm{e}^{-(t/\sigma)^2} \left(\mathrm{e}^{\mathrm{i}t\omega} - \mathrm{e}^{-\sigma^2\omega^2/4} \right), \quad (1)$$

with $\omega = 2\pi$ and $\sigma = 1$. These values provide appropriate resolution in time and period estimates (Soon, Frick & Baliunas 1999).

Then the wavelet transform is defined as

$$W_\tau(t) = \tau^{-1} \int_{t_0}^{t_1} f(t')\, \psi^* \left(\frac{t - t'}{\tau} \right) \mathrm{d}t', \quad (2)$$

and the global wavelet spectrum (corresponding generalization of the Fourier spectrum) is

$$E(\tau) = \tau \int_{t_0}^{t_1} |W_\tau(t)|^2 \mathrm{d}t. \quad (3)$$

Obtaining the global wavelet spectrum (3) from the decomposition (2), we can also perform integration over a specific time interval, say, a particular Schwabe cycle, to get the spectral characteristic of solar activity inside this cycle only. We stress here that this calculation requires the data to be available beyond this particular cycle because equation (2) formally contains the integration over the whole database used. Having wavelet spectra for several Schwabe cycles, we can estimate the standard deviation for the global wavelet spectrum as scattering of wavelet spectra of individual cycles. Below we separate one Schwabe cycle from the next one using the instants at which the corresponding phase of W_{11} (wavelet coefficient at $\tau = 11$) crosses $\pi/2$.

The standard version of wavelet analysis faces problems dealing with gaps and edges in datasets. The problem can be partly resolved with the so-called gapped wavelet algorithm suggested for stellar cyclic activity investigations (Frick, Grossmann & Tchamitchian 1998).

4 RESULTS OF WAVELET ANALYSIS

First we present wavelet spectrograms in the τ-versus-t coordinates, where colour corresponds to the modulus $|W_\tau(t)|$ (Fig. 3). Two pronounced strips at $\tau_1 \approx 11$ yr and $\tau_2 \approx 0.1$ yr can be seen, corresponding to the nominal 11-yr Schwabe cycle and the

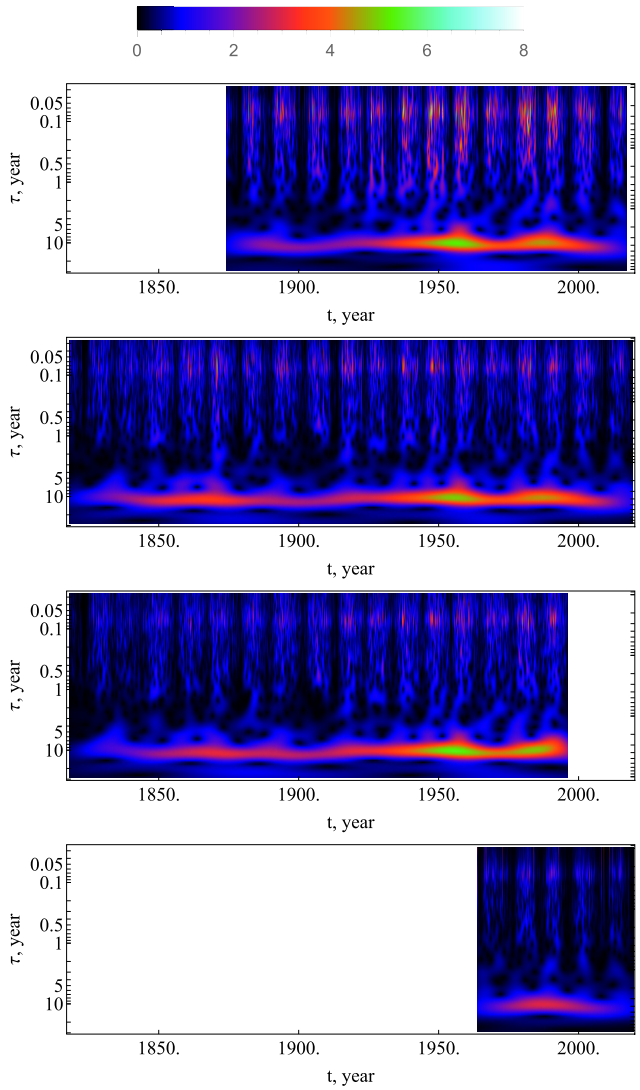

Figure 3. Wavelet spectrograms for SA, SN, GN and F10.7 (from top to bottom). Colours from blue to red correspond to the intensity of $|W_\tau(t)|$.

(synodic) solar rotation period, respectively. Some isolated 'isles' of enhanced power can also be observed between τ_1 and τ_2, i.e. in the frequency/period domain under discussion.

Global wavelet spectra (meaning that integral (3) is taken over the entire length of the time series) are shown in Fig. 4 and display two significant peaks at τ_1 and τ_2. All solar activity indices give very similar global spectra. We also calculated wavelet spectra for GN excluding small (<35 μsd) sunspot groups to verify the robustness of the spectral shape.

The highest peak in the global spectrum is quite broad and corresponds to the nominal 11-yr Schwabe cycle. We note that, since wavelets have a finite spectral resolution, they typically yield a smooth peak even for a purely harmonic signal, as illustrated by the dotted curve in Fig. 4, which corresponds to a purely sinusoidal 11-yr variation.

The second peak is also broad and corresponds to a time-scale of ≈27 d, which is the solar synodic rotation period. This peak is formed by long-lived active regions, whose lifetime exceeds one solar rotation period, and thus they can recurrently contribute to solar activity as traced from the Earth. Since new active regions

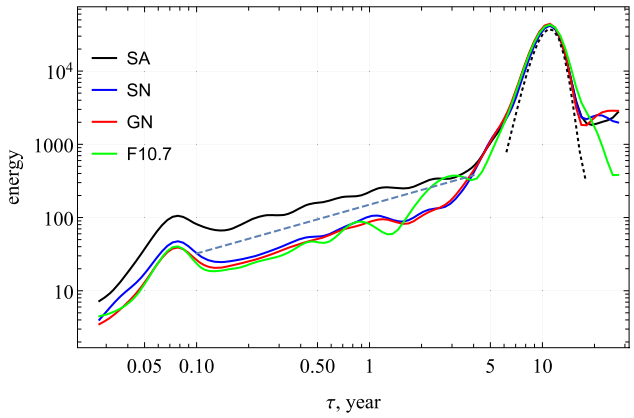

Figure 4. Global wavelet spectra for different tracers: SA (black), SN (blue), GN (red) and F10.7 (green). The dashed line denotes the slope 2/3. The dotted line denotes the response expected from a purely sinusoidal 11-yr signal.

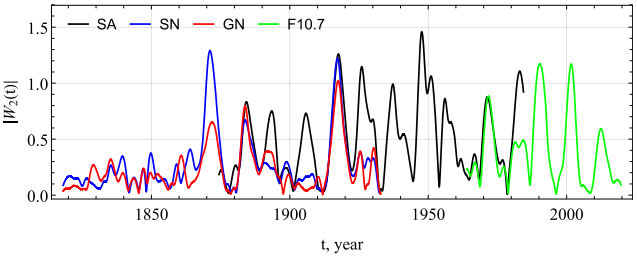

Figure 5. Wavelet amplitude of the 2-yr periodicity (cut off the whole wavelet spectrum) in sunspot data: SA (black), SN (blue), GN (red) and F10.7 (green).

are formed at different latitudes and random longitudes, the peak appears broad. The ability to reproduce the rotational period of solar activity variations is tested below in the framework of a solar dynamo model (Section 5).

The spectrum between these two main periodicities is close to a power law with a slope of about $\tau^{2/3}$. This is in accordance with findings by Plunian, Sarson & Stepanov (2009). We note that a power-law scaling is typical for various convective or turbulent systems. It should also be verified in the framework of dynamo modelling (see Section 5 below).

The time-scale of $\tau \approx 2$ yr related to the QBO (e.g. Bazilevskaya et al. 2014) is not pronounced in the spectra as a separate peak. Of course, the spectrum of sunspot data also contains some power in the QBO: Fig. 5 shows oscillations of the wavelet amplitude of the 2-yr period. One can see that the 2-yr oscillations substantially vary between different tracers, and also in time. For example, relative amplitudes differed by a factor of two during the last five solar circles, when all the considered tracers are available.

The Schwabe cycle is a global feature of the Sun and its convection zone. However, solar activity is not perfectly symmetric between the solar isolated hemispheres. Therefore it is useful to look for a trace of a particular periodicity in each hemisphere separately, as well as in their combination. Thus, we separate the SA dataset into contributions from the Northern (N) and Southern (S) hemispheres and consider their sum $N + S$, i.e. the total signal, and the difference $N - S$, i.e. the excess of the sunspot area in the

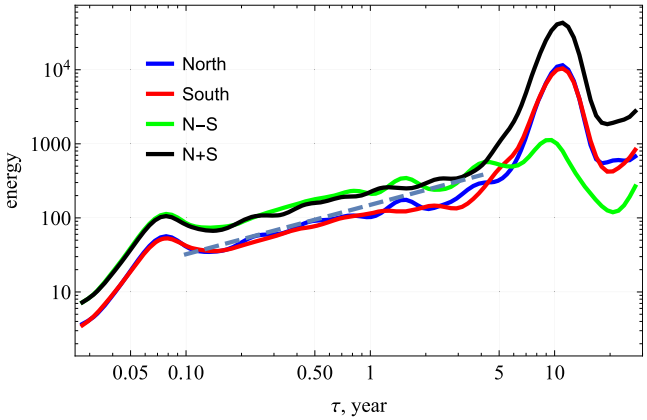

Figure 6. Wavelet spectra for SA with the Northern (blue) and Southern (red) hemispheres considered separately. The green line stands for the $N - S$ data spectrum, while the black one stands for that for the $N + S$ data. The dashed line corresponds to the slope 2/3.

north over the south. The corresponding power spectral densities are shown in Fig. 6. The spectra of separated N and S data subsets are very similar, though a weak peak at $\tau \approx 1.5$ yr occurs in the spectrum of the Northern hemisphere data. The sum $N + S$ and difference $N - S$ allow us to analyse the equatorial (anti)symmetry. Since the Schwabe cycle is produced by a global process, which is symmetric, the power of the corresponding peak in the $N + S$ spectrum is expected to be quadrupole with respect to that of a single hemisphere, while in the $N - S$ spectrum it would become very weak (the contributions of the north and south cancel out). In contrast, the power of the rotation-related peak at about 27 d is equal in both $N + S$ and $N - S$ series. This means that the corresponding variability is provided by isolated (relatively rare) long-lived spots, which occur in both hemispheres independently without correlation and equatorial symmetry. The spectral density between 1 month and 11 yr behaves similarly, supporting the conclusion that this range of frequency is not dominated by global phenomena presented in the Sun as a whole.

Supposing that some additional distinguished periodicity exists in the solar activity spectrum, one should accept the requirement that corresponding oscillations must be pronounced over a few solar cycles. In this case it will be captured by the wavelet spectrum regardless of its appearance with random phase and amplitude. Addressing this point, we analyse the spectral power density cycle by cycle, presenting in Fig. 7 the wavelet spectra for 11 isolated solar cycles, calculated following equation (3), where t_0 and t_1 define the duration of a given cycle. One can see that only two peaks survive over all cycles, while the spectral composition between them varies from cycle to cycle, yielding no stable features. We identified local maxima in the period range from $\tau = 0.2$–4. The middle panel of Fig. 7 shows the relative height of local maxima found in the individual cycle spectrum, with respect to the nearest local minima. One can recognize two high maxima at $\tau = 2$ (in cycle $N = 16$) and $\tau = 2.7$ (in cycle $N = 23$) yr. There are many other slightly less significant maxima that uniformly occur in the mid-term range. We attempt to confirm this in a statistical manner. Fig. 7 (bottom) shows confidence intervals around the mean values obtained by averaging over all the analysed cycles. We can summarize the results of the wavelet analysis as that pronounced oscillations with time-scales between several months and 11 yr are present in each individual cycle. Quite naturally, however, their random contributions yield

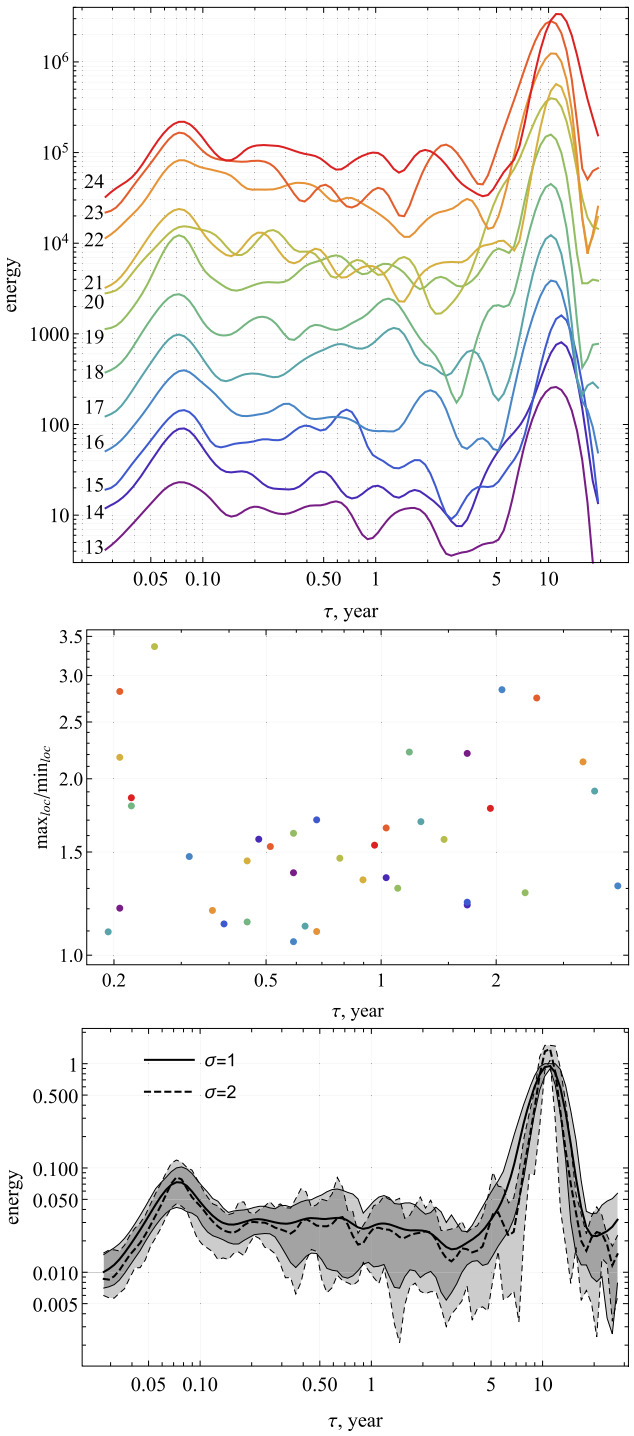

Figure 7. (Top) Wavelet spectra for individual cycles, divided by $\tau^{2/3}$ and scaled by factor $10^{\frac{n-13}{3}}$ (n is the cycle number) for better visualization. (Middle) Local maxima relative to the nearest minima versus their periods for individual cycles. (Bottom) The wavelet spectra averaged over individual Schwabe cycles (individual spectra were rescaled to be the same amplitude at 11 yr and normalized by the power law $\tau^{2/3}$). Grey shading depicts the 80 per cent two-sided confidence interval. Solid and dashed lines correspond to different values of wavelet parameter: $\sigma = 1$ and $\sigma = 2$, respectively.

a smooth overall spectrum. For larger τ, deviations from the simple $\tau^{2/3}$ relation become visible, and the difference from spectra obtained for individual Schwabe cycles becomes larger due to a smaller statistic. We understand this as representing possible isles of intermittent nature in the solar dynamo. Strong intermittency was shown by calculating the corresponding scaling exponents in Plunian et al. (2009). Perhaps the scale of $\tau \approx 2$ yr can be suggested as a time-scale where intermittent effects are substantially pronounced.

5 COMPARISON WITH A SOLAR DYNAMO MODEL

The observed power-law shape of the global wavelet spectra in the period range from 1 month to ≈11 yr (Fig. 6) calls for an interpretation in the framework of relevant dynamo processes operating inside the Sun. Starting from the seminal paper by Parker (1955), it is widely assumed that the surface magnetic activity of the Sun is governed by the cyclic transformation of the large-scale poloidal magnetic field into a toroidal magnetic field by means of differential rotation and turbulent generation of the poloidal magnetic fields from the toroidal magnetic field by small-scale convective cyclic motions. An alternative option for the latter process is mirror asymmetry, which appears due to magnetic force action during sunspot emergence, the so-called Babcock–Leighton scheme, (Charbonneau 2014). Meridional circulation also participates in the process.

The turbulent part of the dynamo process is not well understood. Direct numerical simulations, e.g. Guerrero et al. (2016) and Viviani et al. (2018), can reproduce the cyclic magnetic activity in the form of dynamo waves. However, the properties of the dynamo wave patterns in the models are different from the solar observations. Mean-field models can reproduce the dynamo waves of solar magnetic activity either as a result of magnetic flux transport due the meridional circulation (Charbonneau 2014) or as a result of diffusive dynamo waves from the dynamo distributed over the convection zone (Brandenburg 2005; Pipin & Kosovichev 2011). Those models can explain the axisymmetric components of magnetic activity but they do not take into account the effect of the non-axisymmetric magnetic fields that are produced from the solar active regions emerging and decaying on the solar surface.

Here we apply a dynamo model of Pipin & Kosovichev (2018), which take this process into account using the non-axisymmetric $\alpha^2\omega$ dynamo model. This model is formulated for a non-axisymmetric 3D magnetic field on a sphere using the shallow-water approximation (Dikpati & Gilman 2001). We use the magnetic field decomposition into toroidal and poloidal potentials and their spectral representation via the spherical harmonics. Following the shallow-water approximation it is assumed that the the poloidal part of the magnetic potential is independent of the radial coordinate and the toroidal potential is a linear function of the radius. The dynamo is driven by differential rotation and mirror-asymmetric convection. The effect of turbulence on the evolution of the large-scale magnetic field is parametrized via the mean electromotive force (Krause & Rädler 1980). By construction, this model does not produce mid-term range oscillations. Such oscillations can be connected with sunspot-like activity that induces a non-axisymmetric magnetic field. In order to simulate sunspot formation and induce non-axisymmetric magnetic fields, the model includes the Parker buoyancy, which produces bipolar regions from the toroidal magnetic field at random latitude and time when the magnetic field strength

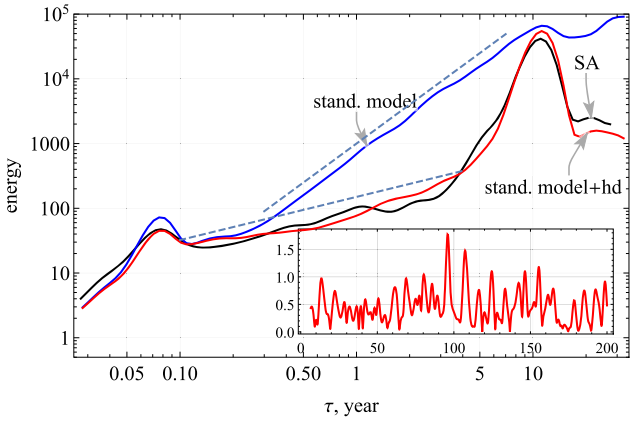

Figure 8. Wavelet spectra for SN (black) and two simulation runs: (blue) standard dynamo model (see Pipin & Kosovichev 2018) and (red) this model with the hyperdiffusion effect. Dashed lines stand for the slopes 2 and 2/3. Inset shows the wavelet amplitude evolution of the 2-yr periodicity (similar to Fig. 5) from data for the model+hd simulation.

exceeds a critical threshold. In this paper we roughly assume that the sunspot production time-scale is about 10 d. More details about the model can be found in Pipin & Kosovichev (2018). The model yields cycles with a mean period of $\approx 0.15\tau^*$ (τ^* being the diffusion time-scale).

Here we used datasets from the dynamo model covering a sequence of 20 dynamo cycles. We have checked that longer simulation does not change the spectral property in the considered range of τ. The signal of magnetic activity produced by the bipolar regions can be used to detect the rotational period. To compare the results of the dynamo model with observations we calculate time series of the magnitude of the total flux of the radial magnetic field averaged over hemisphere (longitudinal range from 0 to π).

A comparison between the wavelet spectra for the simulated and real data is presented in Fig. 8. It is found that with the standard formulation of the model, i.e. the same as in Pipin & Kosovichev (2018), the power spectrum is much steeper ($E(\tau) \sim \tau^2$ in mid-term range) and actually takes up the 11-yr peak (see the blue line labelled 'model' in Fig. 8). We found that short-term fluctuations of the α-effect increase the slope of the spectrum. Next we tested the concept of hyperdiffusion (Δ^2) for a non-axisymmetric magnetic field. In this case the spectrum (the red line in Fig. 8) becomes qualitatively similar to the real solar spectrum. We note that the difference between the simulated ('model+hyperdiff') and real ('SN') spectra is more remarkable near $\tau \approx 2$ yr, but it stays within the confidence intervals in Fig. 7. The inset demonstrates that a signal similar to QBO can appear even in the output of a model, which does not contain such an intrinsic (quasi-)periodicity. Irrespective of the (in)correctness of the model, this implies that QBO (or other mid-term periodicities) can appear as a result of a random realization and/or as an artefact of the analysis method.

It is important for our interpretation that the dynamo model does not contain physical mechanisms that would lead to excitation of any other particular periodicity than the Schwabe cycle. We manage to mimic a peak associated with the solar rotation with special treatment of the simulated data. The results are in good agreement with real data due to sufficiently long-lived surface phenomena and their homogeneous distribution over the surface. The interpretation of the spectrum between these peaks looks natural in the framework of the model under discussion.

6 DISCUSSION AND CONCLUSIONS

The detailed wavelet analysis of available sunspot data that we have performed reveals only two significant periodicities in the frequency/period range between weeks and decades, namely, the solar rotation period and the Schwabe cycle. The latter can be identified with an eigensolution of the solar dynamo, which may be saturated by some non-linear effects. Considering the spectral dynamics of solar activity cycle by cycle, we showed that no particular periodicity can be identified, in a statistically significant manner, in the specified range of periods.

The spectrum in the range of periods between 1 month and 11 yr presumably represents various random components of the solar dynamo system. QBO can be recognized in some individual cycles, but the available data do not provide a basis to identify it with a solar dynamo eigensolution. This implies that there is no need to consider a specific mechanism to explain QBO and it is sufficient to consider it as an element of a continuous spectrum typical for various turbulent convective systems. By comparing the results obtained using different datasets for solar activity, we verified that our results are robust with respect to the choice of dataset.

Moreover, we confirmed that the spectrum in this frequency range is smooth and under reliable statistics tends to be close to the power law $E(\tau) \sim \tau^{2/3}$. This result is important because it allows us to formulate a new criterion for the verification of dynamo models claiming to describe the temporal dynamics of solar activity. Such characteristics (the continuity of the temporal spectrum) have never been considered as a requirement for a dynamo model. In a recent study, Cameron & Schüssler (2019) showed that oscillations with periods longer than the 11-yr solar cycle appear with a overall shape of the power spectrum, which can be well represented by a generic normal form model for a noisy and weakly non-linear limit cycle. This is also in favour of the turbulent nature of the observed solar activity apart from the dominant 11-yr variation.

We examined a relatively simple dynamo model to reproduce the temporal evolution of sunspots. In the framework of the model, active regions are produced by the large-scale dynamo action. In this case non-linear interactions between the large- and small-scale modes of the magnetic field are strong. This can explain the steeper wavelet spectrum for the standard formulation of the model. We found that a realistic spectrum of activity-related characteristics can be obtained if the small spatial (but not temporal) scales are smoothed. In the model this was realized using the concept of hyperdiffusion. In the Sun, the dynamo operates in the depth of the convection zone, and the surface magnetic field represents the decaying part of the dynamo wave. This result is important because solar activity is a *global* feature, although recognized in small-scale tracers like sunspots. Of course, this does not imply that this model adequately reproduces all solar physics that is responsible for sunspot statistics. However, the available data do not allow us to prefer the specific model over the others.

ACKNOWLEDGEMENTS

PF, DS and RS are grateful for the support for this work by the project RSF-Helmholtz (contract nos. 18-41-06201 and HRSF-0044). VP conducted the dynamo model simulations as part of FR II.16 of ISTP SB RAS. IU composed miscellaneous observation data under the support from the Academy of Finland (projects 307411 ReSoLVE and 321882 ESPERA). The dynamo model was tested during the 'Solar Helicities in Theory and Observations:

Implications for Space Weather and Dynamo Theory' programme at the Nordic Institute for Theoretical Physics (NORDITA).

REFERENCES

Ahlers G., Grossmann S., Lohse D., 2009, Rev. Modern Phys., 81, 503
Bazilevskaya G., Broomhall A.-M., Elsworth Y., Nakariakov V. M., 2014, Space Sci. Rev., 186, 359
Benevolenskaya E. E., 1995, Sol. Phys., 161, 1
Bogatyrev G. P., Gilev V. G., Zimin V. D., 1980, JETP Lett., 32, 210
Brandenburg A., 2005, ApJ, 625, 539
Busse F. H., 1983, Phys. D Nonlinear Phenomena, 9, 287
Cameron R. H., Schüssler M., 2019, A&A, 625, A28
Charbonneau P., 2014, ARA&A, 52, 251
Clette F., Lefèvre L., 2016, Sol. Phys., 291, 2629
Dikpati M., Gilman P. A., 2001, ApJ, 551, 536
Dikpati M., McIntosh S. W., Bothun G., Cally P. S., Ghosh S. S., Gilman P. A., Umurhan O. M., 2018, ApJ, 853, 144
Fletcher S. T., Broomhall A.-M., Salabert D., Basu S., Chaplin W. J., Elsworth Y., Garcia R. A., New R., 2010, ApJ, 718, L19
Frick P., Galyagin D., Hoyt D. V., Nesme-Ribes E., Schatten K. H., Sokoloff D., Zakharov V., 1997, A&A, 328, 670
Frick P., Grossmann A., Tchamitchian P., 1998, J. Math. Phys., 39, 4091
Guerrero G., Smolarkiewicz P. K., de Gouveia Dal Pino E. M., Kosovichev A. G., Mansour N. N., 2016, ApJ, 828, L3
Hathaway D. H., 2015, Living Rev. Sol. Phys., 12, 4
Inceoglu F., Simoniello R., Arlt R., Rempel M., 2019, A&A, 625, A117
Krause F., Rädler K.-H., 1980, Mean-field Magnetohydrodynamics and Dynamo Theory. Pergamon Press, New York
Krishnamurti R., Howard L. N., 1981, Proc. Natl. Acad. Sci., 78, 1981
Lawrence J. K., Cadavid A. C., Ruzmaikin A. A., 1995, ApJ, 455, 366
Mallat S., 2008, A Wavelet Tour of Signal Processing, Third Edition: The Sparse Way, 3rd edn. Academic Press, New York
Nesme-Ribes E., Frick P., Sokoloff D., Zakharov V., Ribes J. C., Vigouroux A., Laclare F., 1995, Acad. Sci. Paris Comptes Rendus B Sci. Phys., 12, 525
Niemela J. J., Skrbek L., Sreenivasan K. R., Donnelly R. J., 2001, J. Fluid Mech., 449, 169
Parker E. N., 1955, ApJ, 122, 293
Pipin V. V., Kosovichev A. G., 2011, ApJ, 741, 1
Pipin V. V., Kosovichev A. G., 2018, ApJ, 867, 145
Plunian F., Sarson G. R., Stepanov R., 2009, MNRAS, 400, L47
Qiu X.-L., Tong P., 2001, Phys. Rev. Lett., 87, 094501
Simoniello R., Jain K., Tripathy S. C., Turck-Chièze S., Baldner C., Finsterle W., Hill F., Roth M., 2013, ApJ, 765, 100
Soon W., Frick P., Baliunas S., 1999, ApJ, 510, L135
Usoskin I. G., 2017, Living Rev. Sol. Phys., 14, 3
Usoskin I. G., Kovaltsov G. A., Lockwood M., Mursula K., Owens M., Solanki S. K., 2016, Sol. Phys., 291, 2685
Vaquero J. et al., 2016, Sol. Phys., 291, 3061
Vasiliev A., Sukhanovskii A., Frick P., Budnikov A., Fomichev V., Bolshukhin M., Romanov R., 2016, Int. J. Heat Mass Transfer, 102, 201
Viviani M., Warnecke J., Käpylä M. J., Käpylä P. J., Olspert N., Cole-Kodikara E. M., Lehtinen J. J., Brandenburg A., 2018, A&A, 616, A160
Zaqarashvili T. V., Carbonell M., Oliver R., Ballester J. L., 2010, ApJ, 724, L95
Zimin V. D., Frick P. G., 1988, Turbulent Convection. Nauka, Moscow

This paper has been typeset from a TEX/LATEX file prepared by the author.